

# Robust coherence-based spectral enhancement for speech recognition in adverse real-world environments

Hendrik Barfuss, Christian Huemmer, Andreas Schwarz<sup>1</sup>,  
and Walter Kellermann

*Multimedia Communications and Signal Processing,  
Friedrich-Alexander University Erlangen-Nürnberg,  
Cauerstr. 7, 91058 Erlangen, Germany  
{barfuss,huemmer,schwarz,wk}@lnt.de*

---

## Abstract

Speech recognition in adverse real-world environments is highly affected by reverberation and non-stationary background noise. A well-known strategy to reduce such undesired signal components in multi-microphone scenarios is spatial filtering of the microphone signals. In this article, we demonstrate that an additional coherence-based postfilter, which is applied to the beamformer output signal to remove diffuse interference components from the latter, is an effective means to further improve the recognition accuracy of modern deep learning speech recognition systems. To this end, the 3rd CHiME Speech Separation and Recognition Challenge (CHiME-3) baseline speech enhancement system is extended by a coherence-based postfilter and the postfilter's impact on the Word Error Rates (WERs) of a state-of-the-art automatic speech recognition system is investigated for the realistic noisy environments provided by CHiME-3. To determine the time- and frequency-dependent postfilter gains, we use Direction-of-Arrival (DOA)-dependent and DOA-independent estimators of the coherent-to-diffuse power ratio as an approximation of the short-time signal-to-noise ratio. Our experiments show that incorporating coherence-based postfiltering into the CHiME-3 baseline speech enhancement system leads to a significant reduction of the WERs, with relative improvements of up to 11.31%.

---

<sup>1</sup>A. Schwarz was with the Friedrich-Alexander University of Erlangen-Nürnberg while the work has been conducted. He is now with Amazon Development Center, Aachen, Germany.

*Keywords:* Robust speech recognition, Postfiltering, Spectral enhancement, Coherence-to-diffuse power ratio, Wiener filter

---

## 1. Introduction

For a satisfying user experience of human-machine interfaces it is crucial to ensure a high accuracy in automatically recognizing the user's speech. However, as soon as no close-talking microphone is used for capturing the desired speech signal, the recognition accuracy suffers from additional reverberation, background noise and active interfering speakers which are picked up by the microphones [1, 2]. Techniques for robust speech recognition in such reverberant and noisy environments can be categorized into either front-end (e.g., speech enhancement [3, 4, 5]) or back-end (e.g., acoustic-model adaptation [6, 7, 8]) processing techniques.

The 3rd CHiME Speech Separation and Recognition Challenge (CHiME-3) [9] targets the performance of state-of-the-art Automatic Speech Recognition (ASR) systems in real-world scenarios. The primary goal is to improve the ASR performance of real recorded speech of a person talking to a tablet device in realistic everyday noisy environments by employing front-end and/or back-end signal processing techniques. To this end, a baseline ASR system has been initially provided and updated as follow-up of CHiME-3 to achieve a high recognition accuracy in everyday real-world scenarios. Front-end processing of the updated baseline now employs the BeamformIt toolkit [10] for processing the recorded microphone signals by a Weighted Delay-and-Sum (WDS) beamforming technique. The beamformer output is used as input to the ASR back-end system which contains a Deep Neural Network (DNN)-based acoustic model and a Recurrent Neural Network (RNN)-based language model.

In this article, we extend the updated CHiME-3 baseline system by a low-complexity coherence-based postfilter which is applied to the beamformer output signal to further remove reverberation and non-stationary background noise from the latter. The postfilter is realized as a Wiener filter, where, in contrast

to the classical Wiener filter, see, e.g., [11], we use an estimate of the Coherent-to-Diffuse Power Ratio (CDR) as an approximation of the short-time Signal-to-Noise Ratio (SNR) to compute the time- and frequency-dependent Wiener filter gains. The CDR, which is the ratio of the power of direct and diffuse signal components, needs to be estimated from the microphone signals. We compare and evaluate two Direction-of-Arrival (DOA)-independent and two DOA-dependent CDR estimators. Two of the evaluated CDR estimators have been proposed and shown to be very effective for dereverberation by Schwarz and Kellermann in [12, 13]. The remaining two CDR estimators have been proposed by Jeub et al. [14] and Thiergart et al. [15, 16] earlier than [12, 13], and are evaluated as reference methods. In contrast to the previous work in [12, 13], where the dereverberation performance was evaluated using Word Error Rates (WERs) of a Hidden Markov Model (HMM)-Gaussian Mixture Model (GMM)-based ASR system trained on clean speech, we now evaluate the efficacy of the CDR-based Wiener filter realizations with a state-of-the-art HMM-DNN-based ASR system trained on noisy training data from different acoustic environments (provided by CHiME-3 [9]). Moreover, the new CDR estimators in [12, 13] were proposed and evaluated for a dual-channel microphone array, whereas the recognition task of CHiME-3 involves signal enhancement using a six-channel microphone array. We therefore extended the CDR estimation procedure to a multi-channel (here: six-channel) scenario. To summarize, the contributions of this article are as follows:

1. First-time evaluation of new [12, 13] and previously known [14, 15, 16] CDR estimators with a state-of-the-art HMM-DNN-based ASR system in challenging acoustic scenarios.
2. First-time application of coherence-based dereverberation using the new CDR estimators [12, 13] to a multi-microphone scenario with more than two microphones.

An overview of the signal processing pipeline employed in this work is given in Figure 1. While the purpose of the beamformer is to spatially focus on the tar-

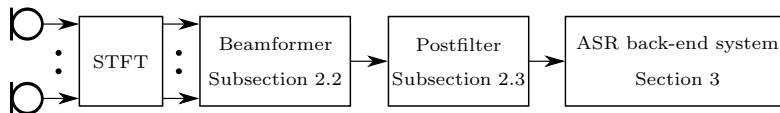


Figure 1: Overview of the overall signal processing pipeline system with beamformer and postfilter as acoustic front-end signal processing. The acoustic back-end system, including feature extraction/transformation, is equal to the updated baseline acoustic back-end system of CHiME-3 (see Section 3 for more details on the employed ASR system).

get source, i.e., to reduce the signal components from interfering point sources, the postfilter shall remove diffuse interference components, e.g., reverberation, from the beamformer output signal. The output of the front-end signal enhancement (consisting of beamformer and postfilter) is further processed by the ASR back-end system, which provides an HMM-DNN-based speech recognizer (see Section 3).

The remainder of this article is structured as follows: In Section 2, the employed front-end signal enhancement is described in detail, followed by a presentation of the employed ASR system in Section 3. Results of our evaluation are presented in Section 4. There, the performance of the front-end speech enhancement using four different CDR estimators is evaluated with respect to WERs of the ASR back-end system. Furthermore, we analyze the statistical significance of the obtained WER improvements. Section 5 provides concluding remarks.

## 2. Front-end enhancement techniques

The front-end speech enhancement considered in this article consists of a WDS beamformer (based on the BeamformIt toolkit [10]) and a single-channel coherence-based Wiener filter. In the following, we introduce the signal model which is used throughout this paper. Then, the baseline WDS beamformer is briefly reviewed, followed by a detailed presentation of the coherence-based Wiener filter based on DOA-independent and DOA-dependent CDR estimation.

### 2.1. Signal model

For a consistent presentation of the front-end speech enhancement, we first introduce a signal model which will be used throughout this article.

The  $N$  microphone signals of the microphone array in the short-time Fourier transform (STFT) domain at frame  $l$  and frequency  $f$  are given as:

$$\mathbf{x}(l, f) = \mathbf{h}(l, f)S(l, f) + \mathbf{n}(l, f), \quad (1)$$

where vector

$$\mathbf{x}(l, f) = [X_0(l, f), X_1(l, f), \dots, X_{N-1}(l, f)]^T \quad (2)$$

contains the microphone signals,  $S(l, f)$  denotes the clean source signal, and  $\mathbf{n}(l, f)$  includes sensor noise as well as interference and diffuse background noise components and is defined analogously to  $\mathbf{x}(l, f)$  in (2). Assuming free-field propagation of sound waves,  $\mathbf{h}(l, f)$  represents the steering vector modeling the sound propagation of a plane wave arriving from the target source DOA  $(\phi_d, \theta_d)$  (azimuth and elevation angle  $\phi$  and  $\theta$  are measured with respect to the positive  $x$ - and  $z$ -axis, respectively, as in [17]) to all  $N$  microphones:

$$\mathbf{h}(l, f) = [e^{j2\pi f\tau_0(l)}, e^{j2\pi f\tau_1(l)}, \dots, e^{j2\pi f\tau_{N-1}(l)}]^T, \quad (3)$$

where  $\tau_n(l)$  is the (possibly time-varying) Time Difference of Arrival (TDOA) for the target source direction of the  $n$ -th channel with respect to the origin of the coordinate system [17]:

$$\tau_n(l) = \frac{\mathbf{a}^T(l)\mathbf{p}_n}{c}. \quad (4)$$

In (4), vector  $\mathbf{p}_n$  contains the position of the  $n$ -th microphone in Cartesian coordinates and the unit vector  $\mathbf{a}(l)$  is defined as [17]:

$$\mathbf{a}(l) = -[\sin(\theta_d)\cos(\phi_d), \sin(\theta_d)\sin(\phi_d), \cos(\theta_d)]^T. \quad (5)$$

Note that  $\mathbf{a}(l)$  points from the target source DOA towards the origin of the coordinate system (hence the minus sign) and that the time-dependency of  $\phi_d$  and  $\theta_d$  in (5) has been omitted for brevity. Moreover,  $c$  represents the

speed of sound and operator  $(\cdot)^T$  denotes the transpose of a vector or matrix. The beamformer output  $Y_{\text{BF}}(l, f)$  is obtained by multiplying each microphone signal with a complex-valued beamformer coefficient  $W_n(l, f)$ , followed by a summation over all microphone channels:

$$Y_{\text{BF}}(l, f) = \mathbf{w}^T(l, f)\mathbf{x}(l, f), \quad (6)$$

where

$$\mathbf{w}(l, f) = [W_0(l, f), \dots, W_{N-1}(l, f)]^T \quad (7)$$

contains the beamformer coefficients  $W_n(l, f)$ .

Subsequently, the postfilter is applied to the beamformer output signal, yielding the overall output signal

$$Y(l, f) = G(l, f)Y_{\text{BF}}(l, f), \quad (8)$$

where  $G(l, f)$  describes the postfilter gain at frame  $l$  and frequency  $f$ . The enhanced signal  $Y(l, f)$  is used as input of the acoustic back-end system (described in Section 3).

## 2.2. Weighted delay-and-sum beamformer

The employed beamformer is provided by the BeamformIt toolkit [10] and based on the WDS beamforming technique [18]. The  $n$ -th beamformer filter coefficient  $W_n(l, f)$  at frame  $l$  and frequency  $f$  is given as

$$W_n(l, f) = w_n(l)e^{-j2\pi f\tau_n(l)}, \quad (9)$$

where  $w_n(l)$  is the frequency-independent weight for the  $n$ -th channel. By modifying  $W_n(l, f)$ , one can control the shape and angular direction of the beamformer's main beam.

The TDOAs are estimated using the Generalized Cross-Correlation with Phase Transform (GCC-PHAT) localization technique, see, e.g., [19]. Before the signals are time-aligned a two-step post processing is applied to the estimated TDOAs: First, a noise threshold is estimated and employed to remove non-reliable TDOA estimates which may have been obtained from non-speech or

noisy segments. Second, Viterbi decoding of the remaining TDOA values is performed to maximize the speaker continuity, i.e., to avoid steering the beam to noise sources which are only present at a very short time span.

The channel weights are chosen adaptively over time, starting with the classical delay-and-sum as initial value:  $W_n(0, f) = 1/N$ . Furthermore, automatic channel selection and elimination is performed to avoid using microphone signals of poor quality. Both, channel weight adaptation and channel selection/elimination are based on the cross-correlations between the microphone channels.

For a more detailed explanation of the baseline beamformer (including localization), as provided by the BeamformIt toolkit, we refer the reader to [10, 20].

### 2.3. Coherence-based postfilter

As illustrated in Figure 1, we apply a postfilter to remove diffuse noise components from the beamformer output signal. The postfilter gain  $G(l, f)$  at frame  $l$  and frequency  $f$  is given as [11, 21]:

$$G(l, f) = \max \left\{ 1 - \mu \frac{1}{1 + \text{SNR}(l, f)}, G_{\min} \right\}, \quad (10)$$

with overestimation factor  $\mu$ , and gain floor  $G_{\min}$ . The postfilter in (10) is a Wiener filter which uses the short-time SNR to compute the filter gain  $G(l, f)$ . In this work, we approximate the short-time SNR in (10) by an estimate of the so-called CDR, which is the power ratio between direct and diffuse signal components. From (10), it can be seen that a low CDR value, which corresponds to strong diffuse signal components being present at the input of the system, leads to low filter gains and vice versa.

The CDR between two omnidirectional microphones is defined as [12]:

$$\text{CDR}(l, f) = \frac{\Gamma_n(l, f) - \Gamma_x(l, f)}{\Gamma_x(l, f) - \Gamma_s(l, f)}, \quad (11)$$

where  $\Gamma_x(l, f)$ ,  $\Gamma_s(l, f)$ ,  $\Gamma_n(l, f)$  denote the coherence functions of the observations, of the direct-path signal, and of the noise between two observation points (microphones), respectively. In the following, the two microphones are indexed

by the variables  $p = 1, \dots, N$  and  $q = 1, \dots, N$ , respectively. To this end, the spatial coherence functions for the direct-path signals and diffuse noise components are given as

$$\Gamma_s(l, f) = e^{j2\pi f(\tau_p(l) - \tau_q(l))}, \quad (12)$$

$$\Gamma_n(f) = \frac{\sin(2\pi f \frac{d_{pq}}{c})}{2\pi f \frac{d_{pq}}{c}}, \quad (13)$$

respectively, with TDOAs  $\tau_p(l)$ ,  $\tau_q(l)$  calculated in (4) and microphone spacing  $d_{pq}$ . Moreover, a short-time estimate  $\hat{\Gamma}_x(l, f)$  of the coherence function of both microphone signals  $\Gamma_x(l, f)$  in (11) can be obtained using

$$\hat{\Gamma}_x(l, f) = \frac{\hat{\Phi}_{x_p x_q}(l, f)}{\sqrt{\hat{\Phi}_{x_p x_p}(l, f) \hat{\Phi}_{x_q x_q}(l, f)}} \quad (14)$$

by estimating the auto- and cross-Power Spectral Densities (PSDs)  $\hat{\Phi}_{x_p x_q}(l, f)$  from the microphone signals  $X_p(l, f)$  and  $X_q(l, f)$  based on recursive averaging

$$\hat{\Phi}_{x_p x_q}(l, f) = \lambda \hat{\Phi}_{x_p x_q}(l-1, f) + (1-\lambda) X_p(l, f) X_q^*(l, f) \quad (15)$$

with forgetting factor  $\lambda$ . Operator  $(\cdot)^*$  creates the conjugate complex of  $(\cdot)$ . However, inserting the coherence estimate  $\hat{\Gamma}_x(l, f)$  into (11) is not feasible due to the mismatch between coherence models and actual acoustic conditions as  $\text{CDR}(l, f)$  might become a complex-valued quantity [13]. Thus, the CDR needs to be estimated. In this work, we use two CDR estimators, which have been proposed and shown to be especially effective in [12, 13], and which are given by

$$\widehat{\text{CDR}}_{\text{DOAindep}} = \max \left( 0, \frac{\Gamma_n \text{Re}\{\hat{\Gamma}_x\} - |\hat{\Gamma}_x|^2 - \sqrt{\Gamma_n^2 \text{Re}\{\hat{\Gamma}_x\}^2 - \Gamma_n^2 |\hat{\Gamma}_x|^2 + \Gamma_n^2 - 2\Gamma_n \text{Re}\{\hat{\Gamma}_x\} + |\hat{\Gamma}_x|^2}}{|\hat{\Gamma}_x|^2 - 1} \right) \quad (16)$$

and

$$\widehat{\text{CDR}}_{\text{DOAdep}} = \max \left( 0, \frac{1 - \Gamma_n \cos(\arg(\Gamma_s))}{|\Gamma_n - \Gamma_s|} \left| \frac{\Gamma_s^* (\Gamma_n - \hat{\Gamma}_x)}{\text{Re}\{\Gamma_s^* \hat{\Gamma}_x\} - 1} \right| \right), \quad (17)$$



respectively, where  $\text{Re}\{\cdot\}$ ,  $|\cdot|$ , and  $\arg\{\cdot\}$  represent the real part, magnitude, and phase of  $(\cdot)$ , respectively. The maximum operation is required to prevent negative results for the CDR estimate. Note that frame- and frequency-index have been omitted in (16) and (17) for brevity. As can be seen from (16), this estimator does not require the TDOA of the target source, since  $\Gamma_s(l, f)$  is not required for calculating  $\widehat{\text{CDR}}_{\text{DOAindep}}$ . This is not the case for the DOA-dependent estimator  $\widehat{\text{CDR}}_{\text{DOAdep}}$  in (17). On the one hand, the advantage of DOA-independent estimators is that these are easier to realize, since no additional information, i.e., the DOA (or TDOA) of the target source, is required. On the other hand, DOA-dependent estimators have a directional filtering effect due to the incorporation of the DOA into the CDR estimate, which is expected to provide a more accurate CDR estimate and, therefore, lead to a better suppression of diffuse noise and reverberation.

In addition to (16) and (17), we evaluate two CDR estimators as reference methods, which have been chosen due to their good speech dereverberation performance in previous experiments [12, 13].

The first reference CDR estimator is a DOA-independent estimator and was proposed by Thiergart et al. in [15, 16]:

$$\widehat{\text{CDR}}_{\text{Thiergart}} = \max \left( 0, \text{Re} \left\{ \frac{\Gamma_n - \hat{\Gamma}_x}{\hat{\Gamma}_x - e^{j \arg \hat{\Gamma}_x}} \right\} \right). \quad (18)$$

This estimator is DOA-independent, because it uses the instantaneous phase of the coherence estimate  $\hat{\Gamma}_x(l, f)$  as phase estimate for the direct signal model, i.e.,  $\hat{\Gamma}_s(l, f) = e^{j \arg \hat{\Gamma}_x(l, f)}$ .

The second reference CDR estimator is based on Jeub's CDR estimator [14]. The estimator is given as:

$$\widehat{\text{CDR}}_{\text{Jeub}} = \max \left( 0, \frac{\Gamma_n - \text{Re}\{\Gamma_s^* \hat{\Gamma}_x\}}{\text{Re}\{\Gamma_s^* \hat{\Gamma}_x\} - 1} \right) \quad (19)$$

and is DOA-dependent. Jeub et al. relied on the same assumption as McCowan and Boulard, who derived a Wiener postfilter for a coherent signal in diffuse noise [22], to explicitly formulate their CDR estimate (19). Hence, (19) can also

be derived using McCowan’s and Boursard’s signal and noise PSD estimates [23].

In [12, 13] it was shown that for non-zero TDOAs both  $\widehat{\text{CDR}}_{\text{Thiergart}}$  and  $\widehat{\text{CDR}}_{\text{Jeub}}$  provide biased CDR estimates, whereas for TDOAs equal to zero, their CDR estimate is unbiased. A more detailed investigation of the employed CDR estimators (16)–(19) with respect to their properties and dereverberation performance for a two-channel microphone array using an HMM-GMM-based ASR system (trained on clean speech) and signal-dependent measures, can be found in [12, 13].

When applying the coherence-based postfilter to the output of a beamformer, two aspects need to be considered: First, since the microphone array of the CHiME-3 challenge consists of five forward-facing microphones (in this work, the additional backward-facing microphone was excluded from the experiments), the CDR estimator (initially designed for a pair of microphones) has to be adapted to exploit all available microphone signals. To do so, we apply the CDR estimators in (16)–(19) to every pair of non-failing microphones (detection and elimination of failing channels is carried out by the BeamformIt toolkit, see Subsection 2.2) to obtain the CDR estimate for each microphone pair.

From each of the CDR estimates, we calculate the respective diffuseness values as [13, 24]

$$D(l, f) = (1 + \widehat{\text{CDR}}(l, f))^{-1}. \quad (20)$$

Subsequently, we take the arithmetic mean of all microphone pair-specific diffuseness values to obtain an average diffuseness estimate  $\overline{D}(l, f)$ . We then calculate the final CDR estimate as:

$$\widehat{\text{CDR}}_{\text{In}}(l, f) = \frac{1 - \overline{D}(l, f)}{\overline{D}(l, f)}. \quad (21)$$

We take the average of the diffuseness estimates instead of averaging the microphone pair-specific CDR values directly, since the latter can take values between zero and infinity, whereas the diffuseness lies in the interval  $0 \leq D(l, f) \leq 1$ . Note that McCowan and Boursard also applied their Wiener postfilter to a multi-microphone setup [22]. The second aspect is that  $\widehat{\text{CDR}}_{\text{In}}(l, f)$  is a CDR

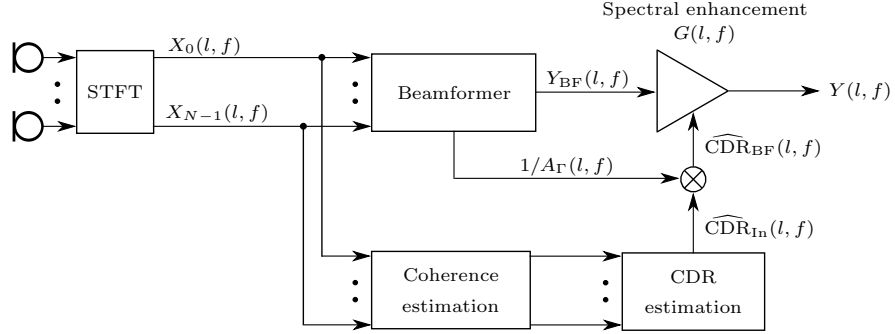


Figure 2: Illustration of the front-end signal processing consisting of beamformer and coherence-based postfilter, where the latter is applied to the beamformer output signal.

estimate at the input of the signal enhancement system, i.e., at the microphones. However, what we need is the CDR at the output of the beamformer. This can be obtained by applying a correction factor  $A_{\Gamma}(l, f)$  to  $\widehat{CDR}_{In}(l, f)$ . Thus, the CDR estimate at the output of the beamformer  $\widehat{CDR}_{BF}(l, f)$  is defined as

$$\widehat{CDR}_{BF}(l, f) = \frac{\widehat{CDR}_{In}(l, f)}{A_{\Gamma}(l, f)}, \quad (22)$$

where  $A_{\Gamma}(l, f)$  is the inverse of the array gain for diffuse noise, given by [25]

$$A_{\Gamma}(l, f) = \mathbf{w}^H(l, f) \mathbf{J}_{\text{diff}}(f) \mathbf{w}(l, f), \quad (23)$$

where  $(\cdot)^H$  denotes the Hermitian of a vector or matrix and  $\mathbf{J}_{\text{diff}}(f)$  is the  $N \times N$  spatial coherence matrix of a diffuse noise field with the  $(p, q)$ -th element given by (13). Note that we assume a distortionless beamformer response for the target source DOA. Hence, the denominator of  $A_{\Gamma}(l, f)$  in (23) is equal to one.

Figure 2 shows the block diagram of the employed front-end enhancement system, consisting of beamformer and coherence-based postfilter. We would like to point out that knowledge of the array geometry is required to estimate the target source TDOAs which are needed to realize the beamformer (9) and the Wiener filter (if one of the DOA-dependent CDR estimators in (17) or (19) is to be used for estimating the CDR).

### 3. ASR back-end system

In this section, we describe the employed ASR back-end system, which was updated by the organizers of CHiME-3 based on the findings of the challenge results. The employed ASR system includes an HMM-GMM system, consisting of 2500 tied triphone HMM states which are modeled by 15000 Gaussians, as well as an HMM-DNN system providing state-of-the-art ASR performance for real-world scenarios. The HMM-DNN system employs a seven-layer feed-forward DNN with 2048 neurons per hidden layer and is based on “Karel’s implementation“ of the Kaldi toolkit [26]. The DNN training process is using noisy data from different acoustic environments and includes pre-training using restricted Boltzmann machines, cross entropy training, and sequence discriminative training using the state-level minimum Bayes risk (sMBR) criterion. We extract 40 Mel-Frequency Cepstral Coefficients (MFCCs) from the single-channel output signal of the acoustic front-end signal enhancement scheme. The resulting length-40 feature vector is passed through per-speaker mean and variance normalization, a feature-space Maximum Likelihood Linear Regression (fMLLR) transformation and context extension, where the latter appends the feature vectors of 3 (HMM-GMM system) or 5 (HMM-DNN system) previous and successive frames. The CHiME-3 baseline system performs acoustic front-end signal enhancement during training and decoding (i.e., we train on enhanced features obtained from the output signals of the acoustic front-end including beamforming and postfiltering). In the decoding phase, we produce word lattices (3-gram language model), generate a 100-best list (5-gram language model) and perform lattice rescoring using an RNN-based language model (one hidden layer with 300 nodes) trained on the WSJ0 text corpus. More details about the RNN-based language modeling can be found in [27].

### 4. Experiments

In the following, we evaluate the signal enhancement performance of our proposed front-end (see Figure 2) consisting of WDS beamforming and coherence-

based postfiltering. First, we give an overview over the evaluation setup and the choice of front-end parameters. After this, we illustrate the impact of the proposed front-end enhancement on the STFT spectra of a noisy speech utterance. Finally, we evaluate the speech recognition accuracy achieved by the HMM-DNN-based ASR system presented in Section 3 using our proposed signal enhancement described in Section 2, and verify the statistical significance of the obtained WER improvements.

#### 4.1. Setup and parameters

To obtain the STFT-representation, we use a Discrete Fourier Transform (DFT)-based uniform filterbank with window length 1024, Fast Fourier Transform (FFT) size 512, and downsampling factor 128 [28]. The signals were processed at a sampling rate of 16 kHz. DOA estimation and WDS beamforming were provided by the BeamformIt toolkit. The window and scroll sizes used for BeamformIt were the default baseline parameters, i.e., 500ms and 250ms, respectively. The array geometry was known a priori.

For realizing the coherence-based postfilter, we chose a gain floor  $G_{\min} = 0.1$  and optimized the overestimation factor  $\mu$  on the development data set (see Figure 5). The short-time coherence estimates  $\hat{\Gamma}_x(l, f)$  were obtained by recursive averaging of the auto- and cross-PSDs with forgetting factor  $\lambda = 0.68$  in (15).

The ASR task included sets of real and simulated noisy utterances in four different environments: café (CAF), street junction (STR), public transport (BUS), and pedestrian area (PED). For each environment, a training set, a development set, and an evaluation set consisting of real and simulated data were provided by CHiME-3 [9]. The training data set consists of 1600 real and 7138 simulated utterances from a total of four (real), and 83 (simulated) speakers. The development data set contains 1640 real and simulated utterances, whereas the evaluation data set consists of 1320 real and simulated utterances. The utterances within each data set were obtained from different speakers. In this work, we focused on evaluating the recognition accuracy of the DNN-based ASR

system for the practically relevant case of real-world recordings.

#### 4.2. Illustration of front-end impact in the STFT domain

In Figure 3, an exemplary illustration of the impact of our proposed front-end, including WDS beamformer and coherence-based postfilter with overestimation factor  $\mu = 1.3$  (at this point,  $\mu$  was chosen according to [13]), on the STFT spectra of a noisy utterance is shown, with frame  $l$  and frequency  $f$  on the horizontal and vertical axis, respectively. The coherence-based postfilter was realized using the DOA-dependent CDR estimator in (17). As a reference signal, the spectrum of the close-talking microphone (channel 0) is shown in Figure 3(a). It contains the desired speech signal plus little background noise. The desired signal is a male speaker saying “*Our guess is no*” in a café environment. The spectrum of microphone channel 1 is illustrated in Figure 3(b). As can be seen, low- as well as high-frequency noise is acquired by the microphone, whereas most of the noise is present in the frequency range of speech. Applying the baseline beamformer already leads to a reduction of the interfering components, as illustrated in Figure 3(c). A thorough comparison of Figure 3(c) with Figure 3(d) shows that applying the coherence-based postfilter to the beamformer output further reduces the interference across the entire frequency range. The estimated diffuseness  $\bar{D}(l, f)$  at the microphones is illustrated in Figure 3(e). Comparing Figure 3(e) with the spectrogram of the reference signal in 3(a) shows that  $\bar{D}(l, f)$  exhibits low values whenever the target source is active and a comparison to 3(c) and 3(d) shows that the dereverberation effect is most prominent where diffuseness is high. Furthermore, it can be seen that  $\bar{D}(l, f)$  is large whenever the target source is not active, indicating a high level of diffuse noise components. A final comparison of Figures 3(a) and 3(d) reveals the similarity between the front-end output signal  $Y(l, f)$  and the close-talking microphone signal  $S(l, f)$ , which indicates the effectiveness of the proposed front-end signal enhancement technique.

In Figure 4, we illustrate the estimated diffuseness  $\bar{D}(l, f)$  obtained with the DOA-dependent estimator (17) in Figure 4(b) and with the DOA-independent

estimator (16) in Figure 4(c), to highlight the difference between our two estimators. As a reference, the spectrogram of the reference signal is shown in Figure 4(a), again. It can be seen that both estimators yield an estimated diffuseness with a similar structure, i.e., the diffuseness is of low value when the target signal is active and vice versa. However, it can be seen that the DOA-dependent estimator in general attributes higher diffuseness values to time-frequency regions where the target signal is not active. The reason for this difference lies in the fact that the DOA-dependent estimator exhibits a directional filtering effect, whereas the DOA-independent estimator does not. The DOA-dependent estimator only considers signal components arriving from the given target DOA as desired signal components, while directional signal components from other directions will increase the diffuseness estimate. Consequently, the DOA-dependent estimator will lead to stronger suppression in time-frequency regions where the target signal is not active. Even if no directional interferers are present, the DOA-dependent estimator can achieve higher suppression of diffuse noise due to lower sensitivity to the variance of the coherence estimate for diffuse signal components [29].

#### 4.3. Evaluation of recognition accuracy

In the following, we evaluate the recognition accuracy obtained by the front-end signal enhancement in Section 2 combined with the ASR system in Section 3. More precisely, we evaluate the impact of coherence-based single-channel Wiener filtering, realized using ...

- DOA-independent CDR estimation (16), termed  $WF_{\text{DOAindep}}$ ,
- DOA-dependent CDR estimation (17), termed  $WF_{\text{DOAdep}}$ ,
- DOA-independent CDR estimation (18), termed  $WF_{\text{Thiergart}}$ ,
- DOA-dependent CDR estimation (19), termed  $WF_{\text{Jeub}}$ .

In Figure 5, the resulting WERs for real recordings of the CHiME-3 development set are illustrated for different values of the overestimation factor  $\mu$  in

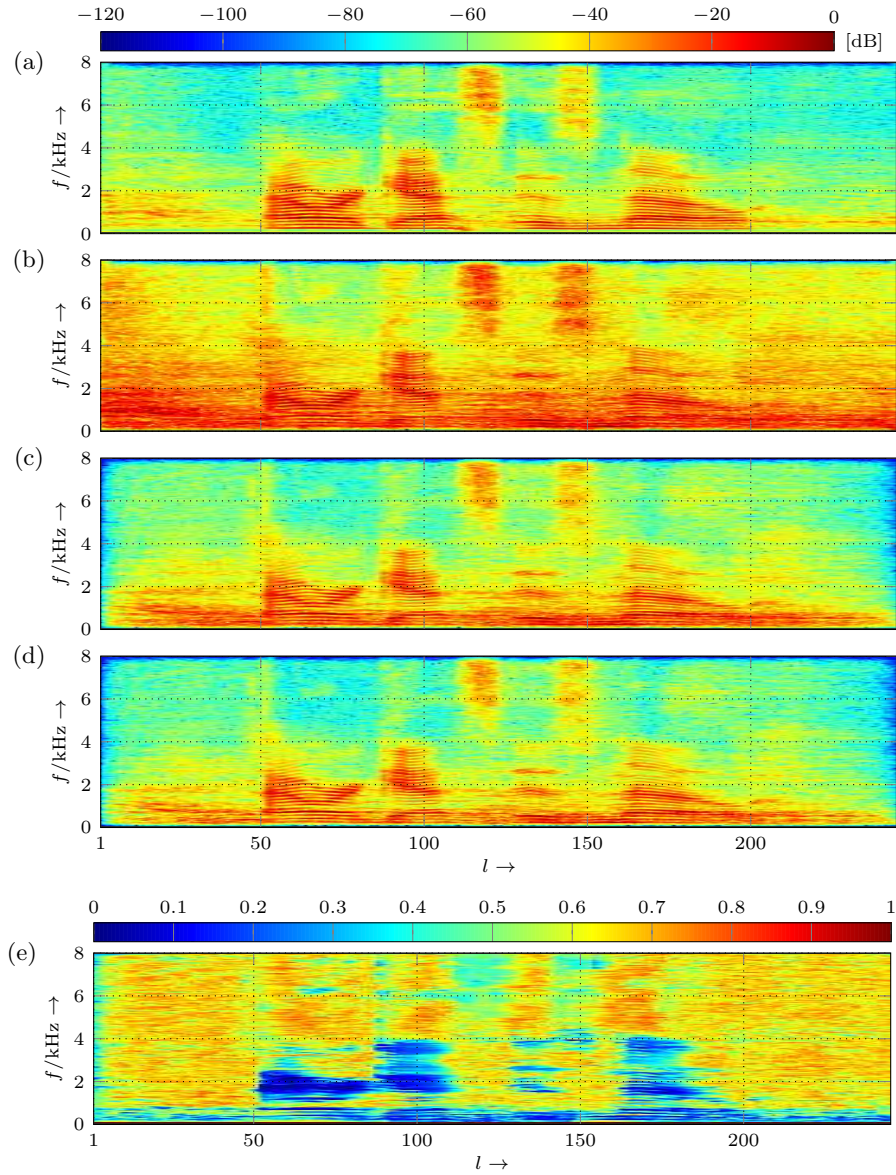


Figure 3: Illustration of the impact of front-end signal processing on the recorded noisy microphone signal. Spectrograms of (a) desired signal  $20 \log_{10}(|S(l, f)|)$ , recorded by a close-talking microphone, of (b) microphone signal  $20 \log_{10}(|X_1(l, f)|)$ , of (c) baseline beamformer output signal  $20 \log_{10}(|Y_{BF}(l, f)|)$ , and of (d) postfilter output signal  $20 \log_{10}(|Y(l, f)|)$  based on the DOA-dependent CDR estimator in (17). Figure (e) shows the average diffuseness  $\bar{D}(l, f)$ , estimated from the microphone signals.



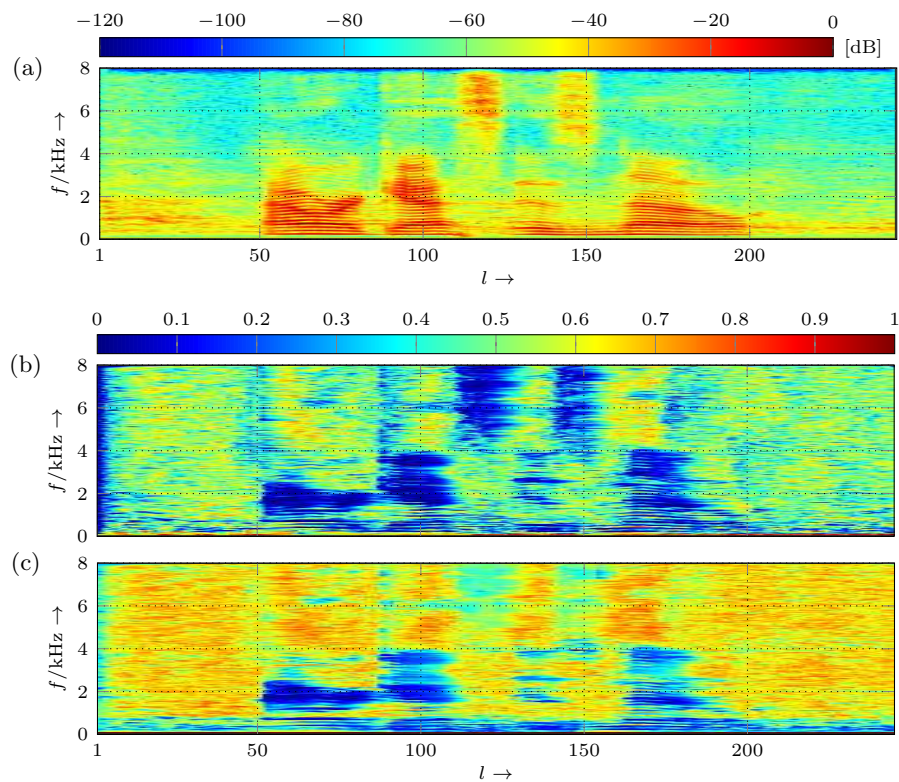


Figure 4: Comparison of the behaviour of the two different CDR estimators in (16) and (17). Figure (a) shows the spectrogram of the recorded close-talking signal  $20 \log_{10}(|S(l, f)|)$ . Figures (b) and (c) show the average diffuseness, estimated using the DOA-independent and DOA-dependent estimator in (16) and (17), respectively.

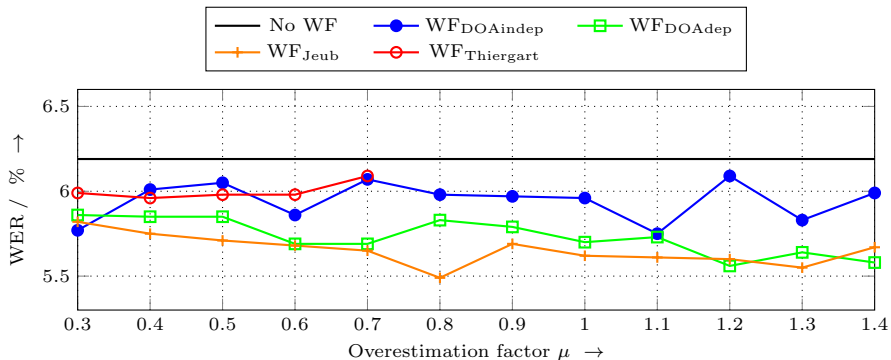


Figure 5: WERs obtained by the CHiME-3 ASR system for real recordings of the development set without (“No WF”) and with coherence-based postfiltering of the beamformer output signal using DOA-independent (WF<sub>DOAindep</sub> and WF<sub>Thiergart</sub>) and DOA-dependent (WF<sub>DOAdep</sub> and WF<sub>Jeub</sub>) CDR estimation.

(10). It is obvious that the recognition accuracy of the CHiME-3 ASR system without postfilter (“No WF” in Figure 5) is consistently improved by incorporating coherence-based postfiltering, except for WF<sub>Thiergart</sub> with  $\mu \geq 0.8$  which yielded WERs between 6.45% and 7.94%. Since these WERs are higher than those without postfiltering, they are not shown in Figure 5 to allow for a clearer presentation of the remaining results. Moreover, it can be seen from Figure 5 that the Wiener filters which were realized using DOA-dependent CDR estimators (WF<sub>DOAdep</sub> and WF<sub>Jeub</sub>) yield a better signal enhancement performance compared to Wiener filters realized using DOA-independent CDR estimators (WF<sub>DOAindep</sub> and WF<sub>Thiergart</sub>). Among the DOA-dependent Wiener filter realizations, WF<sub>Jeub</sub> yields a slightly better performance than WF<sub>DOAdep</sub> for almost every value of  $\mu$ .

Based on the results illustrated in Figure 5, we selected one overestimation factor  $\mu_{opt}$  for each Wiener filter realization, in order to obtain the best performance in the experiments using the evaluation data set (real data). The selected overestimation factors for each Wiener filter realization are summarized in Table 1. One can see that the overestimation factors chosen for WF<sub>Thiergart</sub> and WF<sub>Jeub</sub> are much smaller than those for WF<sub>DOAindep</sub> and WF<sub>DOAdep</sub>. To verify

Table 1: Selected overestimation factors  $\mu_{\text{opt}}$  for which each Wiener filter realization achieved the best signal enhancement performance for the real recordings of the CHiME-3 development data set.

	$\text{WF}_{\text{DOAindep}}$	$\text{WF}_{\text{DOAdep}}$	$\text{WF}_{\text{Thiergart}}$	$\text{WF}_{\text{Jeub}}$
$\mu_{\text{opt}}$	1.1	1.2	0.4	0.8

that there is no unfair comparison of the different Wiener filter realizations due to the potentially lower noise suppression performance, we also evaluated the real recordings of the evaluation data set for the different overestimation factors. Our results showed that larger overestimation factors as the ones in Table 1 for  $\text{WF}_{\text{Thiergart}}$  and  $\text{WF}_{\text{Jeub}}$  do not lead to better WERs for these Wiener filter realizations.

In Table 2, the average WERs (averaged over all environment-specific WERs) for the CHiME-3 development and evaluation set (both real data) obtained with the CHiME-3 ASR system without (“No WF”) and with coherence-based post-filtering of the beamformer output signal using DOA-independent ( $\text{WF}_{\text{DOAindep}}$  and  $\text{WF}_{\text{Thiergart}}$ ) or DOA-dependent ( $\text{WF}_{\text{DOAdep}}$  and  $\text{WF}_{\text{Jeub}}$ ) CDR estimation are compared. Moreover, the relative WER improvements with respect to the baseline signal enhancement (without postfilter) are given. The results show that the coherence-based postfiltering of the beamformer output signal consistently improves the recognition accuracy of the ASR system for both, the development set as well as the evaluation set. For the development set,  $\text{WF}_{\text{Jeub}}$  yields the lowest WER, closely followed by  $\text{WF}_{\text{DOAdep}}$ , with relative WER improvements with respect to the baseline signal enhancement of 11.31% and 10.18%, respectively. On the contrary, for the evaluation data set  $\text{WF}_{\text{DOAdep}}$  performs best, followed by  $\text{WF}_{\text{DOAindep}}$ . Here, the average WER of the baseline signal enhancement is reduced by up to 8.21%.

To provide more insight into the behavior of the various Wiener filter realizations in the different acoustic environments provided by CHiME-3, we provide the environment-specific WERs obtained for the evaluation set (real data) in

Table 3. We observe that except for the STR environment,  $WF_{DOAdep}$  always yields the best results. In the STR environment,  $WF_{DOAindep}$  proves to be slightly better. The latter might be due to incorrectly localized target source directions in this environment.

In order to investigate the statistical significance of the WER improvements obtained with the various Wiener filter realizations for the real evaluation data set, we applied the Matched-Pair Sentence-Segment Word Error (MAPSSWE) test to the results in Table 2. The MAPSSWE test uses knowledge of aligned reference and hypothesis (produced by the ASR system) sentence strings to locate segments within the sentence strings which contain misclassified content. To compare two different systems, the number of errors in each segment for each system is computed, and the null hypothesis that the mean difference in the number of word errors per segment between the two systems is zero is tested, see, e.g. [30, 31]. In our experiments, a significance level of  $p = 5\%$ , i.e., a 95% confidence level for rejecting the null hypothesis, was chosen. We used the implementation of the MAPSSWE test provided by the National Institute of Standards (NIST) Scoring Toolkit [32]. Table 4 compares the results of the MAPSSWE test. For every comparison, the better signal enhancement system is given in the corresponding field of the table if a statistically significant difference between the systems was found, and “same” otherwise. All Wiener filter realizations yield a statistically significant improvement of the signal enhancement baseline without postfiltering of the beamformer output signal. It can furthermore be observed that  $WF_{DOAdep}$  performs significantly better than  $WF_{Thiergart}$  and  $WF_{Jeub}$ , but no significant difference between  $WF_{DOAdep}$  and  $WF_{DOAindep}$  is found. Thus, a consistent and statistically significant benefit of exploiting DOA information for CDR-based postfiltering cannot be inferred from the results. An additional significance test for the results of the different Wiener filter realizations for the real development data set did also not show a consistent and statistically significant advantage of DOA-dependent over DOA-independent CDR-estimators.

Table 2: Average WERs and relative WER improvements (in %) for the CHiME-3 development and evaluation set (both real data) obtained with the CHiME-3 ASR system without (“No WF”) and with coherence-based postfiltering of the beamformer output signal using DOA-independent ( $WF_{DOAindep}$  and  $WF_{Thiergart}$ ) and DOA-dependent ( $WF_{DOAdep}$  and  $WF_{Jeub}$ ) CDR estimation. The relative WER improvements are given with respect to the WER of the baseline signal enhancement.

	Development set		Evaluation set	
	avg. WER	rel. Impr.	avg. WER	rel. Impr.
No WF	6.19	-	12.67	-
$WF_{DOAindep}$	5.75	7.10	11.78	7.02
$WF_{DOAdep}$	5.56	10.18	<b>11.63</b>	<b>8.21</b>
$WF_{Thiergart}$	5.96	3.71	12.16	4.03
$WF_{Jeub}$	<b>5.49</b>	<b>11.31</b>	12.13	4.26

Table 3: Environment-specific WERs (in %) for the CHiME-3 evaluation set (real data) obtained with the CHiME-3 ASR system without (“No WF”) and with coherence-based postfiltering of the beamformer output signal using DOA-independent ( $WF_{DOAindep}$  and  $WF_{Thiergart}$ ) and DOA-dependent ( $WF_{DOAdep}$  and  $WF_{Jeub}$ ) CDR estimation.

	Evaluation set			
	BUS	CAF	PED	STR
No WF	18.53	11.39	10.50	10.27
$WF_{DOAindep}$	17.71	9.71	9.79	<b>9.88</b>
$WF_{DOAdep}$	<b>17.42</b>	<b>9.36</b>	<b>9.57</b>	10.18
$WF_{Thiergart}$	18.70	10.07	9.98	9.90
$WF_{Jeub}$	18.47	9.73	10.05	10.25

Table 4: Comparison matrix showing results of the MAPSSWE test applied to the results of the various front-end signal enhancement algorithms for the evaluation set (real data). For the MAPSSWE test a significance level of  $p = 5\%$  was used.

	$WF_{DOAindep}$	$WF_{DOAdep}$	$WF_{Thiergart}$	$WF_{Jeub}$
No WF	$WF_{DOAindep}$	$WF_{DOAdep}$	$WF_{Thiergart}$	$WF_{Jeub}$
$WF_{DOAindep}$		same	same	same
$WF_{DOAdep}$	same		$WF_{DOAdep}$	$WF_{DOAdep}$
$WF_{Thiergart}$	same	$WF_{DOAdep}$		same
$WF_{Jeub}$	same	$WF_{DOAdep}$	same	

## 5. Conclusion

We proposed to extend the front-end speech enhancement of a state-of-the-art ASR system by coherence-based postfiltering of the beamformer output signal. The postfilter is realized as a Wiener filter, where an estimate of the power ratio between direct and diffuse signal components at the output of the beamformer is used as an approximation of the short-time SNR to compute the time- and frequency-dependent postfilter gains. To estimate the ratio between direct and diffuse signal components, we used two DOA-independent and two DOA-dependent estimators, which can be efficiently realized by estimating the auto- and cross-PSDs at the microphone signals. As a consequence, the postfilter has a very low computational complexity. Baseline and extended front-end speech enhancement have been evaluated on real recordings provided by CHiME-3 with respect to WERs of a state-of-the-art HMM-DNN-based ASR system. The results confirmed that coherence-based postfiltering in general improves the recognition accuracy of the ASR system significantly, with relative improvements of up to 11.31% and 8.21% for the development and the evaluation data set, respectively. Consistent statistically significant differences between Wiener filters based on DOA-independent and DOA-dependent CDR

estimators could not be observed. The improved recognition accuracy in addition to the low computational complexity makes coherence-based postfiltering very suitable for real-time robust distant speech recognition. As future work, it should be evaluated whether CDR-based postfilters for dereverberation still yield a significant improvement of WERs when a more powerful beamforming algorithm is used: On the one hand, if the beamformer has a higher directivity, i.e., a higher suppression of diffuse noise components, a CDR-based postfilter might be less effective because the beamformer partly fulfills the function of the CDR-based postfilter. On the other hand, if the beamformer already partly suppresses the diffuse noise, then the postfilter sees a better input CDR and could possibly be tuned to be more aggressive, which could further improve speech recognition performance. Another aspect of future work is the investigation of the combination of DOA-independent and DOA-dependent CDR estimators in different frequency areas, in order to obtain an even better diffuseness estimate.

## 6. Acknowledgement

We would like to thank Stefan Meier and Christian Hofmann for their continuous support and fruitful discussions.

The research leading to these results has received funding from the European Union's Seventh Framework Programme (FP7/2007-2013) under grant agreement n° 609465 and from the Deutsche Forschungsgemeinschaft (DFG) under contract number KE 890/4-2.

## References

- [1] M. Delcroix, Y. Kubo, T. Nakatani, A. Nakamura, Is speech enhancement pre-processing still relevant when using deep neural networks for acoustic modeling?, in: Interspeech, 2013, pp. 2992–2996.
- [2] T. Yoshioka, M. Gales, Environmentally robust ASR front-end for deep neural network acoustic models, *Computer Speech and Language (CSL)* 31 (1) (2015) 65–86.

- [3] I. Cohen, Noise spectrum estimation in adverse environments: improved minima controlled recursive averaging, *IEEE Trans. Speech Audio Process.* (SAP) 11 (5) (2003) 466–475.
- [4] A. Krueger, R. Haeb-Umbach, Model-based feature enhancement for reverberant speech recognition, *IEEE Trans. Audio, Speech Lang. Process.* (ASLP) 18 (7) (2010) 1692–1707.
- [5] M. Gales, Y.-Q. Wang, Model-based approaches to handling additive noise in reverberant environments, in: *Proc. IEEE Joint Workshop Hands-free Speech Comm. Microphone Arrays (HSCMA)*, IEEE, 2011, pp. 121–126.
- [6] X. Li, J. Bilmes, Regularized adaptation of discriminative classifiers, in: *Proc. IEEE Int. Conf. Acoustics, Speech, Signal Process. (ICASSP)*, IEEE, 2006, pp. 237–240.
- [7] H. Liao, Speaker adaptation of context dependent deep neural networks, in: *Proc. IEEE Int. Conf. Acoustics, Speech, Signal Process. (ICASSP)*, IEEE, 2013, pp. 7947–7951.
- [8] D. Yu, K. Yao, H. Su, G. Li, F. Seide, KL-divergence regularized deep neural network adaptation for improved large vocabulary speech recognition, in: *Proc. IEEE Int. Conf. Acoustics, Speech, Signal Process. (ICASSP)*, IEEE, 2013, pp. 7893–7897.
- [9] J. Barker, R. Marxer, E. Vincent, S. Watanabe, The third ‘CHiME’ speech separation and recognition challenge: Dataset, task and baselines., in: *IEEE Workshop Automat. Speech Recog., Understanding (ASRU)*, IEEE, 2015, pp. 504–511.
- [10] X. Anguera, C. Wooters, J. Hernando, Acoustic beamforming for speaker diarization of meetings, *IEEE Trans. Audio, Speech Lang. Process.* (ASLP) 15 (7) (2007) 2011–2022.



- [11] E. J. Diethorn, *Acoustic signal processing for telecommunication*, Kluwer Academic Publishers, Hingham, MA, USA, 2000, Ch. Subband Noise Reduction Methods for Speech Enhancement, pp. 155–179.
- [12] A. Schwarz, W. Kellermann, Unbiased coherent-to-diffuse ratio estimation for dereverberation, in: *Proc. IEEE Int. Workshop Acoustic Echo, Noise Control (IWAENC)*, IEEE, 2014, pp. 6–10.
- [13] A. Schwarz, W. Kellermann, Coherent-to-diffuse power ratio estimation for dereverberation, *IEEE Trans. Audio, Speech Lang. Process. (ASLP)* 23 (6) (2015) 1006–1018.
- [14] M. Jeub, C. M. Nelke, C. Beaugeant, P. Vary, Blind estimation of the coherent-to-diffuse energy ratio from noisy speech signals, in: *Proc. 19th European Signal Processing Conference (EUSIPCO)*, 2011, pp. 1347–1351.
- [15] O. Thiergart, G. Del Galdo, E. Habets, Signal-to-reverberant ratio estimation based on the complex spatial coherence between omnidirectional microphones, in: *Proc. IEEE Int. Conf. Acoustics, Speech, Signal Process. (ICASSP)*, IEEE, 2012, pp. 309–312.
- [16] O. Thiergart, G. Del Galdo, E. Habets, On the spatial coherence in mixed sound fields and its application to signal-to-diffuse ratio estimation, *J. Acoust. Soc. Am. (JASA)* 132 (2012) 2337.
- [17] H. Van Trees, *Optimum Array Processing, Detection, Estimation, and Modulation Theory*, Wiley, 2004.
- [18] B. D. V. Veen, K. M. Buckley, A versatile approach to spatial filtering, *IEEE ASSP Magazine* 5 (2) (1988) 4–24.
- [19] M. S. Brandstein, H. F. Silverman, A robust method for speech signal time-delay estimation in reverberant rooms, in: *Proc. IEEE Int. Conf. Acoustics, Speech, Signal Process. (ICASSP)*, IEEE, 1997, pp. 375–378.

- [20] X. Anguera, Robust speaker diarization for meetings, Ph.D. thesis, UPC Barcelona (2006).
- [21] E. Haensler, G. Schmidt, Acoustic Echo and Noise Control: A Practical Approach, Wiley-Interscience, 2004.
- [22] I. McCowan, H. Bourlard, Microphone array post-filter based on noise field coherence, *IEEE Trans. Speech Audio Process. (SAP)* 11 (6) (2003) 709–716.
- [23] A. Schwarz, A. Brendel, W. Kellermann, Coherence-based dereverberation for automatic speech recognition, in: *Deutsche Jahrestagung für Akustik (DAGA)*, Oldenburg, Germany, 2014, pp. 525–526.
- [24] G. Del Galdo, M. Taseska, O. Thiergart, J. Ahonen, V. Pulkki, The diffuse sound field in energetic analysis, *J. Acoust. Soc. Am. (JASA)* 131 (3) (2012) 2141–2151.
- [25] K. U. Simmer, J. Bitzer, C. Marro, Post-filtering techniques, in: *Microphone Arrays, Digital Signal Processing*, Springer Berlin Heidelberg, 2001, pp. 39–60.
- [26] D. Povey, A. Ghoshal, G. Boulianne, L. Burget, O. Glembek, N. Goel, M. Hannemann, P. Motlicek, Y. Qian, P. Schwarz, The Kaldi speech recognition toolkit.
- [27] T. Hori, Z. Chen, H. Erdogan, J. R. Hershey, J. L. Roux, V. Mitra, S. Watanabe, The MERL/SRI system for the 3rd CHiME challenge using beamforming, robust feature extraction, and advanced speech recognition, in: *IEEE Workshop Automat. Speech Recog., Understanding (ASRU)*, IEEE, 2015, pp. 475–481.
- [28] M. Harteneck, S. Weiss, R. W. Stewart, Design of near perfect reconstruction oversampled filter banks for subband adaptive filters, *IEEE Transactions on Circuits and Systems II: Analog and Digital Signal Processing* 46 (8) (1999) 1081–1085.

- [29] C. Zheng, A. Schwarz, W. Kellermann, Statistical analysis and improvement of coherent-to-diffuse power ratio estimators for dereverberation, in: Proc. IEEE Int. Workshop Acoustic Echo, Noise Control (IWAENC), IEEE, 2016, pp. 1–5.
- [30] L. Gillick, S. J. Cox, Some statistical issues in the comparison of speech recognition algorithms, in: Proc. IEEE Int. Conf. Acoustics, Speech, Signal Process. (ICASSP), IEEE, 1989, pp. 532–535.
- [31] D. S. Pallet, W. M. Fisher, J. G. Fiscus, Tools for the analysis of benchmark speech recognition tests, in: Proc. IEEE Int. Conf. Acoustics, Speech, Signal Process. (ICASSP), IEEE, 1990, pp. 97–100.
- [32] N. I. of Standards (NIST), NIST scoring toolkit, version 2.4.10 (Aug. 2016). URL <https://github.com/chinshr/sctk>